INTERNATIONAL JOURNAL FOR NUMERICAL METHODS IN FLUIDS, VOL. 20, 853–868 (1995)

ENTROPY CORRECTING SCHEMES AND NON-HIERARCHICAL AUTO-ADAPTIVE DYNAMIC FINITE ELEMENT-TYPE MESHES: APPLICATIONS TO UNSTEADY AERODYNAMICS

ROLAND RICHTER AND PÉNÉLOPE LEYLAND

Institut de Machines Hydrauliques et Mécanique des Fluides Ecole Polytechnique Fédérale de Lausanne, CH-1015 Lausanne, Switzerland

SUMMARY

This paper discusses the different sources of non-physical entropy production which occur in the numerical resolution of the Euler equations for compressible inviscid flow and proposes several ways of correcting these effects. In particular a hybrid corrected centred, augmented by an accurate upwind scheme near singular boundaries is proposed which satisfies the mathematical entropy condition, and which solves the flow accurately within regions near non-smooth boundaries of the computational domain. A coupled new dynamic auto-adaptive mesh algorithm which produces highly accurate solutions is also introduced. This algorithm is non-hierarchical, i.e. it does not depend on a fixed background mesh, which allows structural and geometrical changes and generates extremely precise discretizations for steady and unsteady flow.

KEY WORDS: numerical schemes; non-linear hyperbolic systems; Reimann solvers; adaptive meshes; unsteady flows

1. INTRODUCTION

Numerical simulation of complex steady and unsteady compressible flows require schemes that are able to capture the different types of discontinuities within the field, and accurately represent the flow behaviour near boundaries. Non-physical solutions of hyperbolic systems, such as the non-linear system of the Euler equations for compressible flow, which can also be seen as the convective kernel of the complete Navier–Stokes equations, can be avoided by ensuring an entorpy preserving property of the designed schemes.[1] Another anomaly pertaining to the relative dissipative nature of the numerical schemes is the spurious non-physical entropy production which can arise in the vicinity of solid wall boundaries presenting non-continuous discretization contours, and geometrical singularities. This is due to the incapacity of such schemes in solving exactly the cell interface problems within such regions. This provokes a non-physical boundary layer-type phenomenon which can lead to sources of non-physical vorticity downstream and forbid accurate capturing of near wall contact discontinuities. The entropy preserving property is not satisfied immediately by many popular numerical schemes which need to be corrected in order to do so.[2,3] However, the near-wall boundary problem implies entropy losses which are not taken into account by such corrections, and a localized hybridzation of schemes in such zones is investigated in order to obtain precise solutions at a reduced cost compared to full non-linear Riemann solvers. The numerical dissipative nature of the numerical schemes also plays an

CCC 0271–2091/95/080853–16

important role in the control of such questions, whether it is explicit as in artificial viscosity methods or internal as for approximate Riemann solvers, for instance.

The ability of the underlying numerical scheme to correctly and precisely represent the different physical processes within the flow field is also highly linked to the grid structure of the discretization. This can be considerably enhanced by using adapted grids. Indeed, precise simulation of unsteady aerodynamic configurations can be performed with a high level of accuracy and efficiency by use of auto-adaptive dynamic mesh procedures. The framework of unstructured meshes is particularly relevant for implementing such algorithms. Adaptation of the current mesh to the flow field is obtained by local mesh enrichment and coarsening by removing superfluous nodes. Combining the relative grid dependency of the numerical scheme and auto-adaptive grids using refinement–derefinement algorithms on unstructured meshes provides a robust tool for capturing sharply defined physical phenomena, as for instance, shock formations, moving free surfaces, reaction zones or flame propagation in combustion. Also, these methods provide a remeshing strategy for unsteady flows, allowing a specific physical phenomena to be 'followed' with accuracy. For example, multiple shock reflections in air engine inlets or turbo-machinary cascades, provide difficult cases of unsteady flow, with not only strong shock interactions, but also secondary transient shocks and contact discontinuities.

In this paper, the possibility of correcting simplified numerical schemes with entropy corrections and using a hybrid scheme near discontinuous surfaces are discussed and tested for unsteady transient shock problems. Comparison with approximate Riemann solvers are given. Generic external and internal unsteady aerodynamical problems are solved by use of auto-adaptive dynamical mesh adaptation. The algorithms developed here use a non-hierarchical data structure which allows greater freedom for optimising the quality of the generated meshes, with a gain in memory and CPU requirements.

2. NUMERICAL METHOD

2.1. Governing equations

The Euler equations for compressible flow form a hyperbolic system of conservation laws which can be written in two dimensions as

$$\begin{aligned} &\frac{\partial \mathbf{W}}{\partial t} + \frac{\partial \mathbf{F}_1(\mathbf{W})}{\partial x} + \frac{\partial \mathbf{F}_2(\mathbf{W})}{\partial y} = 0 \quad \text{for } (x, y, t) \in \Omega \times \mathbb{R}^+ \\ &\mathbf{W}(x, y, 0) = \mathbf{W}_0(x, y) \quad \text{for } (x, y) \in \Omega \\ &\text{plus appropriate boundary conditions} \quad \text{for } (x, y, t) \in \Gamma \times \mathbb{R}^+ \end{aligned} \tag{1}$$

where

$$\mathbf{W} = \begin{pmatrix} \rho \\ \rho u \\ \rho v \\ \rho E \end{pmatrix}; \quad \mathbf{F}_1 = \begin{pmatrix} \rho u \\ \rho u^2 + p \\ \rho uv \\ u(\rho E + p) \end{pmatrix}; \quad \mathbf{F}_2 = \begin{pmatrix} \rho v \\ \rho uv \\ \rho v^2 + p \\ v(\rho E + p) \end{pmatrix}$$

ρ designates the density, (u, v) the speed, p the pressure, and E total energy. The system is closed by a state equation relating the pressure to the total energy, which for a perfect gas gives

$$p = (\gamma - 1)\left(\rho E - \rho \frac{u^2 + v^2}{2}\right)$$

The Euler equations only have weak global solutions, which implies that strong gradients and discontinuities, such as shock waves, expansion fans and contact discontinuities are present within the admissible solutions. In order to filter out amongst the multiple solutions the physical solutions an *entropy preserving* condition is enforced following Lax.[1]

Definition

An *entropy* function is a convex function $\mathscr{W}(\mathbf{x}.t)\colon \mathbb{R}^{d+2} \to \mathbb{R}$, such that there exists an *entropy flux* $\mathscr{F}(\mathbf{W}) = [\mathscr{F}_1(\mathbf{W}), \ldots, \mathscr{F}_d(\mathbf{W})]$, with

$$\frac{\mathrm{d}\mathscr{W}(\mathbf{W})}{\mathrm{d}\mathbf{W}} \frac{\mathrm{d}\mathbf{F}_k(\mathbf{W})}{\mathrm{d}\mathbf{W}} = \frac{\mathrm{d}\mathscr{F}_k(\mathbf{W})}{\mathrm{d}\mathbf{W}}, \quad k = 1, \ldots, d$$

The weak solution $\mathbf{W}(x,t)$ of (1) satisfies the *entropy condition* if for all entropy functions, $\mathscr{W}(\mathbf{x},t)$, corresponding to the entropy flux $\mathscr{F}(\mathbf{W})$, then the following inequality is satisfied:

$$\frac{\partial \mathscr{W}(\mathbf{W})}{\partial t} + \sum_{k=1}^{d} \frac{\partial \mathscr{F}_k(\mathbf{W})}{\partial \mathbf{x}_k} \leqslant 0$$

in the sense of measures.

In particular for the Euler equations of gas dynamics, $\mathscr{W}(\mathbf{W}) = -\rho h(s)$, $\mathscr{F}(\mathbf{W}) = -\rho \mathbf{u} h(s)$, where $s = \ln(p/\rho^{\gamma})$ is the physical entropy. For $d \geqslant 2$, the existence of an entropy couple, $(\mathscr{W}, \mathscr{F})$ can be related to the fact that the system is symetrizable via a change of variables, $\mathbf{W} = \hat{\mathbf{W}}(\mathscr{V})$. Formulations of the Euler equations in terms of entropy variables enforces naturally the second principle of thermodynamics.[4] The above entropy condition can again be expressed in terms of these entropy variables.

2.2. *Numerical approximation*

The numerical methods employed here are based upon a spatial approximation using the hybrid Galerkin finite volume method on the 'dual' control volumes of the underlying P1 Galerkin finite element approximation. These cells constitute the dual topology of the $P1$ triangular n-simplex space, such that the finite volume formulation over the dual cells is equivalent to a $P1$ Galerkin finite element approximation.[5,6] They are constructed by taking the barycentres of the contributing triangles to a discretization node i, as in the Figure 1. The Galerkin finite volume method is based upon the variational form of the equations (1).

Let $\mathscr{V} = \{v \in C^0(\mathbf{\Omega}),\ v|_T \text{ linear } \forall T \in \mathscr{T}\}$ (P_1-approximation)

$$\text{Find } \mathbf{W} \in \mathscr{V}^4 \text{ such that } \forall \varphi \in \mathscr{V},$$

$$\int_{\Omega} \frac{\partial \mathbf{W}}{\partial t} \varphi_i \, \mathrm{d}\mathbf{\Omega} = -\sum_{j \in k(i)} \int_{\partial \mathscr{C}_{ij}} \mathbf{F}(\mathbf{W}) \cdot \mathbf{n}_{ij} \, \mathrm{d}\sigma - \int_{\partial \mathscr{C}_i \cap \Gamma} \mathbf{F}(\mathbf{W}) \cdot \mathbf{n}_{\Gamma} \, \mathrm{d}\sigma \tag{2}$$

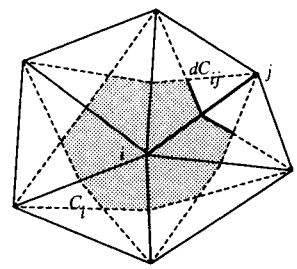

Figure 1. Construction of a dual cell

$\partial\mathscr{C}_{ij}$ denotes the interface boundary of the dual cell around the node i with respect to a neighbouring node j.

The numerical scheme is defined by the numerical flux function $\mathbf{\Phi}_{\mathbf{F}_{ij}}$ in the direction of the normal $\mathbf{n}_{ij}$ to the cell interface between states i and j:

$$\int_{\partial\mathscr{C}_{ij}} \mathbf{F}(\mathbf{W})\cdot\mathbf{n}_{ij}\,\mathrm{d}\sigma = \mathbf{\Phi}_{\mathbf{F}_{ij}}(\mathbf{W}_i, \mathbf{W}_j)$$

Any such numerical flux may be written formally as

$$\mathbf{\Phi}_{\mathbf{F}_{ij}}(\mathbf{W}_i, \mathbf{W}_j) = \tfrac{1}{2}[\mathbf{F}(\mathbf{W}_i) + \mathbf{F}(\mathbf{W}_j)] + \mathbf{\Phi}^{*}_{\mathbf{F}_{ij}}(\mathbf{W}_i, \mathbf{W}_j) \tag{3}$$

where $\mathbf{\Phi}^{*}_{\mathbf{F}_{ij}}(\mathbf{W}_i, \mathbf{W}_j)$ represents the dissipative part of scheme. This numerical dissipation is either artificial viscosity terms or an implicit dissipation.

Here, two such numerical fluxes are considered, a standard centred difference flux with additional artifical dissipation for stability and shock-capturing of the Jameson type, and the Osher flux which is an approximate Riemann solver.

For the centred scheme both a second-order and fourth-order artificial dissipation are necessary. These terms are calculated in a way similar to finite difference stencils as illustrated in the Figure 2:

$$\mathbf{\Phi}^{*}_{\mathbf{F}_{ij}}(\mathbf{W}_i, \mathbf{W}_j) = \tilde{\lambda}_{ij}\varepsilon^{(2)}_{ij} D^{(2)}(\mathbf{W}_i, \mathbf{W}_j) - \tilde{\lambda}_{ij}\varepsilon^{(4)}_{ij} D^{(4)}(\mathbf{W}_{i^*}, \mathbf{W}_i, \mathbf{W}_j, \mathbf{W}_{j^*})$$

The shock capturing second-order term contains a TVD pressure switch, and the fourth-order term for high-frequency damping is scaled to mutually exclude regions of high second-order disspation. For details on these dissipation terms we refer to References 7–9.

The Osher flux can be written formally as

$$\mathbf{\Phi}(\mathbf{W}_i, \mathbf{W}_j) = \tfrac{1}{2}\left[\mathbf{F}_{ij}(\mathbf{W}_i) + \mathbf{F}_{ij}(\mathbf{W}_j) - \int_{\mathbf{W}_i}^{\mathbf{W}_j} |\mathbf{A}_{ij}(\mathbf{W})|\,\mathrm{d}\mathbf{W}\right]$$

where the integral depends on the choice of integration path Γ between the states W_i and W_j, $\Gamma = \Gamma_1 \cup \Gamma_2 \cup \Gamma_3$, corresponding to two compression waves for the truely non-linear fields and a contact discontinuity for the linearly degenerate field. Second-order accuracy is obtained by a third-order MUSCL extrapolation which renders an overall second-order accuracy for irregular meshes with a minmod limiter near discontinuities.

The system (2) leads to a set of coupled ordinary differential equations of the form

$$\frac{\mathbf{W}_i^{n+1} - \mathbf{W}_i^{n}}{\mathrm{d}t} + \Sigma^{-1}\mathbf{R}(\mathbf{W}_i) = \mathbf{0} \quad \text{with } \Sigma = \mathbf{diag}\left[\frac{\text{aire}(\mathscr{C}_i)}{\Delta t^n}\right] \tag{4}$$

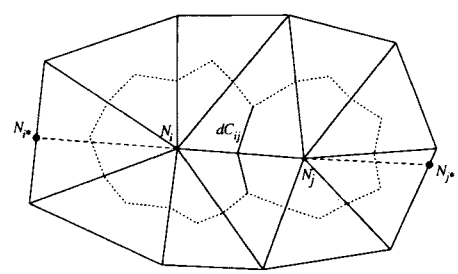

Figure 2. Construction of points i^* and j^*

Time integration is performed by a four stage Runge–Kutta integration procedure, assuring good time accuracy and stability properties for both unsteady and steady-state situations.

$$\bar{\mathbf{W}}_i^{(0)} \overset{\text{def}}{=} \mathbf{W}_i^n$$

$$\bar{\mathbf{W}}_i^{(k)} = \bar{\mathbf{W}}_i^{(0)} - \alpha_k \boldsymbol{\Sigma}^{-1} \mathbf{R}(\bar{\mathbf{W}}_i^{(k-1)}) \quad \text{for } k = 1, \ldots, m$$

$$\mathbf{W}_i^{n+1} \overset{\text{def}}{=} \bar{\mathbf{W}}_i^{(m)}$$

where α_k are taken to be standard coefficients.[10]

2.3. *Discrete entropy condition*

The above centred scheme has the advantages to be straightforward to implement and very efficient in CPU time requirements. However its main drawback is the presence of serious entropy oscillations in strong gradient regions due to the non-preservation of the entropy condition, and also non-physical entropy production at solid wall boundaries, particularly near sharp changes of the geometry (see examples below). The first point can be rectified by adding an entropy correction similar to that proposed by References 2 and 11. This correction is discussed briefly below.

Following the notation of Reference 12 , a general numerical flux in two dimensions (3) can be written as an explicit plus a dissipation part plus an implicit part. For the explicit part in two space dimensions:

$$\Delta \mathbf{W}_i^{\text{exp}} = -(\sigma_1 \delta_1 \boldsymbol{\Phi}_1 + \sigma_2 \delta_2 \boldsymbol{\Phi}_2)_i$$

with the following notation, $\boldsymbol{\Phi}_{k=1,d} = (\boldsymbol{\Phi}_1, \ldots, \boldsymbol{\Phi}_d)$, $d = 2$ and μ_k, δ_k are average and difference operators.

$$\Delta \mathbf{W} \equiv \mathbf{W}^{n+1} - \mathbf{W}^n, \quad \delta \mathscr{A} = (\mathscr{A}_j - \mathscr{A}_i), \quad \mu \mathscr{A} = \tfrac{1}{2}(\mathscr{A}_i + \mathscr{A}_j), \quad \sigma_k = \frac{\Delta t}{\Delta x_k}.$$

The discrete entropy inequality becomes

$$(\sigma_1 \delta_1 \boldsymbol{\Theta}_1 + \sigma_2 \delta_2 \boldsymbol{\Theta}_2)_i \leqslant 0$$

where $(\boldsymbol{\Theta}_1, \boldsymbol{\Theta}_2)$ is the numerical entropy flux consistent with $(\mathscr{F}_1, \mathscr{F}_2)$. In terms of the entropy variables $\mathscr{V}$ this flux can be written as $\boldsymbol{\Theta} = \mu \mathscr{F} + \mu \mathscr{V}^{\mathrm{T}} \boldsymbol{\Phi} - \mu(\mathscr{V}^{\mathrm{T}} \mathbf{F})$. The explicit numerical flux is thus modified in the following way:

$$\tilde{\boldsymbol{\Phi}}_k^{\text{exp}} = \boldsymbol{\Phi}_k^{\text{exp}} - \tfrac{1}{2} \beta_k \delta \mathbf{W} \quad \text{with } \beta_k = \begin{cases} 0 & \text{if } \vartheta = 0 \\ \chi \dfrac{\max(q_k^*, 0)}{\vartheta_k} & \text{otherwise} \end{cases}$$

and

$$\vartheta = (\delta \mathscr{V}^{\mathrm{T}} \delta W)$$

$$\left.\begin{aligned} q_x^* &= 2\sigma_x [\delta \mathscr{F}_1 - (\mu \mathscr{V})^{\mathrm{T}} \delta \mathbf{F}_1] \\ q_y^* &= 2\sigma_y [\delta \mathscr{F}_2 - (\mu \mathscr{V})^{\mathrm{T}} \delta \mathbf{F}_2] \end{aligned}\right\} \text{ and } \chi \geqslant 1$$

This term acts in fact as an anti-diffusion flux, which can be added to the original second-order difference dissipative flux. Its role is in fact to adjust the dissipation in such a way that the entropy overshoots and undershoots near discontinuities become physical.

The entropy production near discontinuous boundaries is not resolved in this way as the mathematical entropy condition is not violated in the flow downstream of the discontinuous wall zone (entropy losses). The break in the boundary provokes a compression wave, a numerical and a physical mini-expansion fan. The above entropy correction cannot compensate for the spurious entropy layer coming from the numerics and the centred scheme cannot cope with the interface problems localized in these zones, whereas a Riemann solver automatically solves the problem correctly. In the example illustrated in the Figure 3, an unsteady supersonic flow at Mach 3 over a forward step of height 0·2 in a channel of height 1, is considered. This test case has been used as a benchmark for testing different dissipation and entropy control of different numerical methods.[3] The centred scheme violates the entropy condition near shocks as shown by the oscillations within the shocks, and presents a strong non-physical entropy production at the singular corner, this creates 'boundary layer' phenomena downstream along the wall boundary, as clearly visible within the iso-Mach or iso-entropy lines. If no particular correction is applied, this scheme does not converge at all to a physical possible solution (Figure (3, *top left*)). For this reason a hybrid Centred/Riemann scheme is proposed. Within regions of discontinuous boundaries and for a certain number of cells downstream of this region the numerical flux is evaluated by the approximate Riemann solver. The adaptation of the standard centred scheme increases of course the CPU cost, but it still results a reduction of more than 50 per cent compared to calculation performed completely with a non-linear approximate Riemann scheme (see Table I). The implemenetation of the hybrid scheme depends on a search algorithm for discontinuous boundaries, and a systematic flagging of neighbouring cells. The interface cell between the two numerical fluxes remains consistent with the approximation, over the dual control volumes, as each subsection of the boundary between to such adjacent cells is treated with one single flux term.

One, unacceptable, way of getting around this problem is to locally refine intensively the singular point of the corner, and coarsen the mesh downstream, thus minimizing the effect of entropy production. However, a locally refined/derefined adaptive mesh algorithm will allow us to follow the evolution of the solution over the corner. Indeed, by dynamically adapting the mesh using the procedures detailed in the next section, the number of nodes necessary for a precise solution with the proposed hybrid scheme can even be considerably reduced (more than a third in this case), and the accuracy of the solution is even improved, as illustrated by the Figure 4.

Table I. Normalized CPU time and MFLOPS rate

Solver	CPU seconds	CPU normalized	Megaflops
Centred scheme	125	1	135
Corrected centred scheme	354	2·8	160
Corrected hybrid scheme	437	3·5	170
Osher	1303	10·4	180

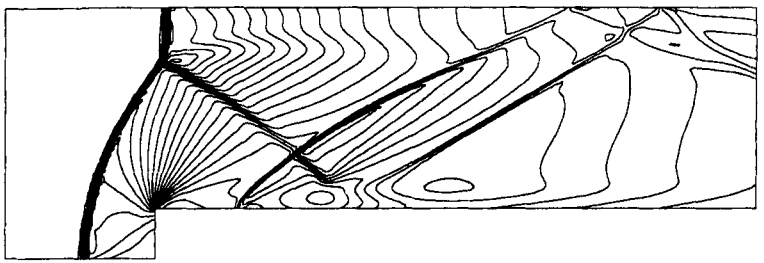

Instantaneous density contour lines at $t^* = 4.0$ obtained with a Standard centered type scheme : the solution is false.

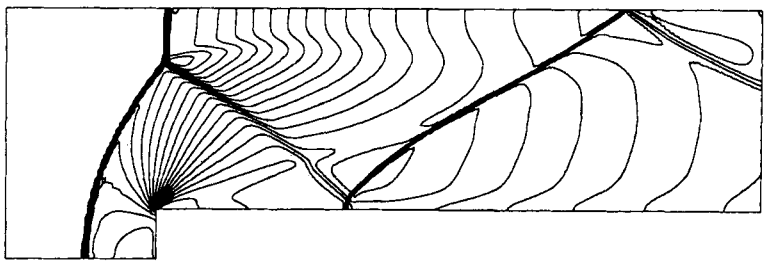

Density contour lines obtained with an approximate Riemann Solver (Osher Scheme).

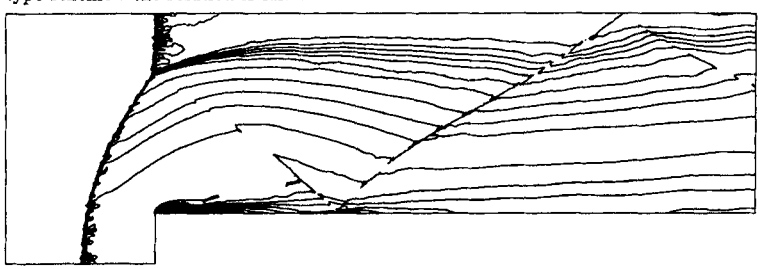

Entropy contour lines, corrected centered scheme with Riemann solver at boundaries.

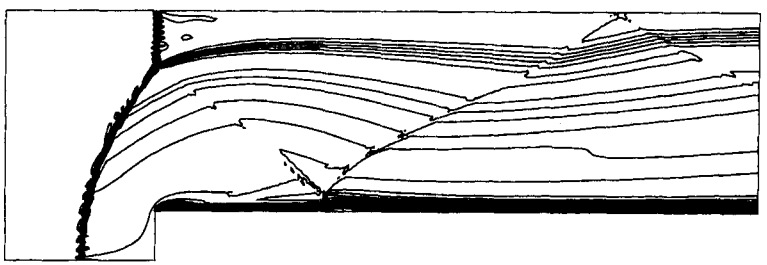

Entropy lines with for the Non-Corrected Centered Scheme

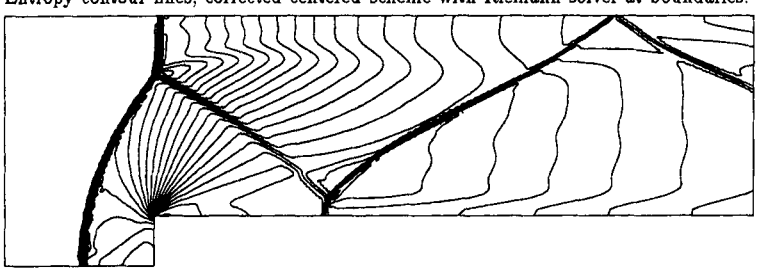

Density contour lines obtained with a centered type scheme corrected by an Osher scheme on the boundaries.

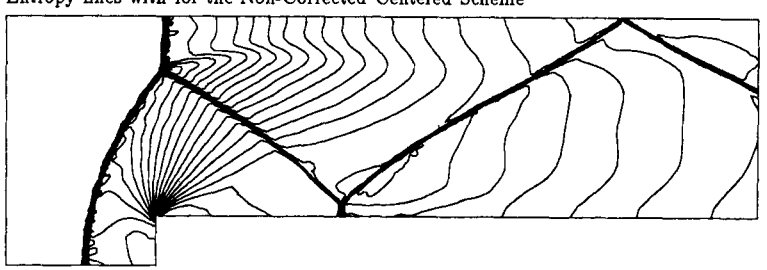

Density contour lines obtained on the adapted mesh with a centered type scheme corrected by an Osher scheme on the boundaries.

Figure 3. Comparison of schemes for the unsteady flow over a forward step at Mach 3, for $t^* = 3{\cdot}5$

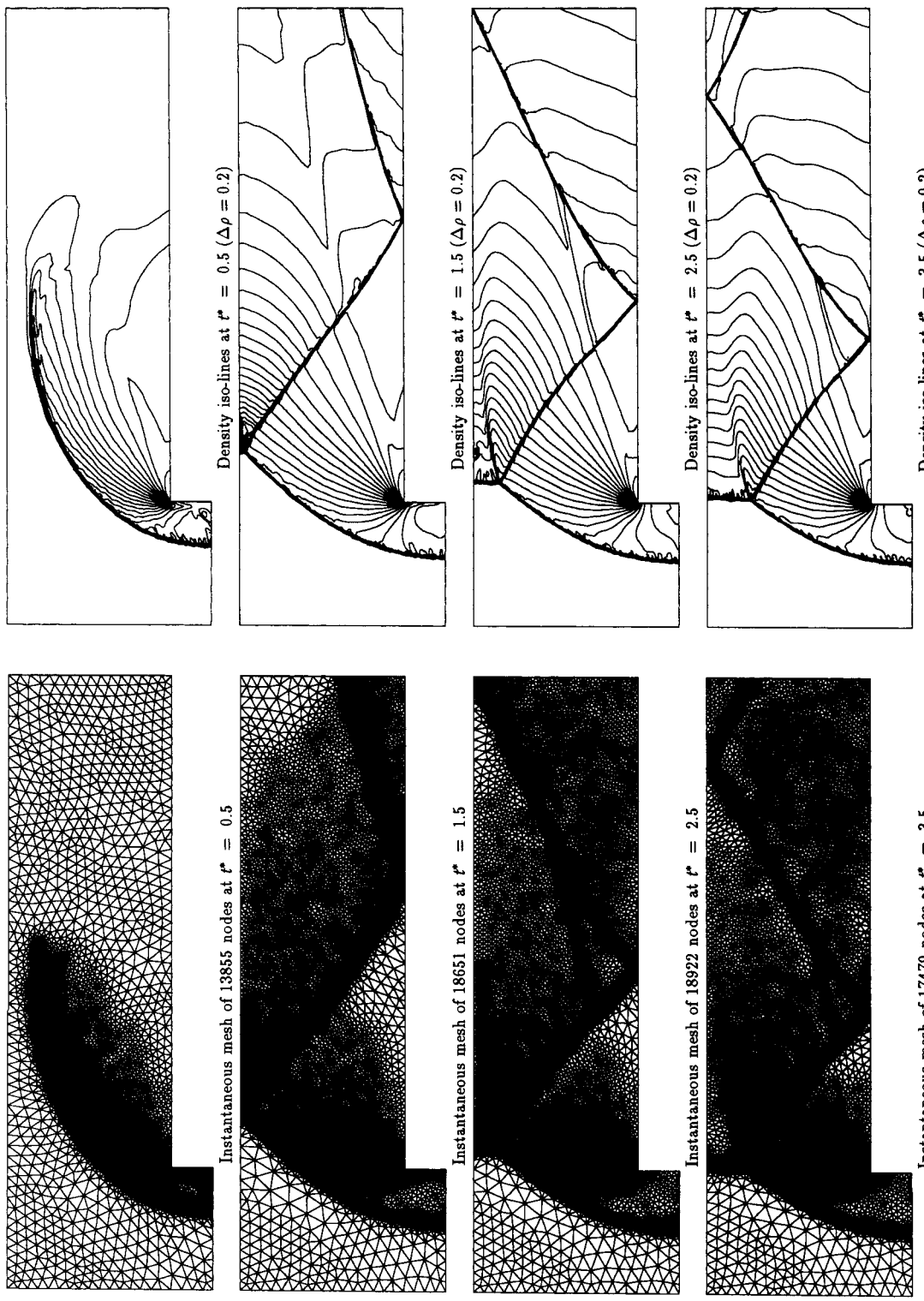

Figure 4. Mesh and solution evolution enabled by dynamic mesh adaption for a forward step at Mach 3

3. MESH ADAPTATION ALGORITHMS

3.1. Motivation

One of the most important advantages of unstructured grids is the possibility to refine/derefine locally the mesh during the computation. Successive mesh concentration by local refinement in critical zones may be performed, without knowing these zones *a priori* at the initial mesh creation time, as well as mesh derefinement which can be performed in regions where the nodes seem superfluous. Hence the overall the amount of discretization nodes is reduced to an optimal relation between precision and calculation cost (CPU time and memory constraint). Strong physical gradients and other characteristic phenomena can be tracked within the flow field by higher grid point concentrations. This is especially important for unsteady flows. In low supersonic flows, as for instance inlet geometries, the interesting regions are the shock waves and the expansion fans, which have to be precisely located and well quantified. Localized refinements are obtained in such zones, which are determined precisely by the combination of several physical criteria, such as shock sensors, density discontinuities and strong gradients.

The mesh adaptation procedure is automatically coupled wihin the solution algorithm. The refinement/derefinement process is made hierarchically free by use of internal flagging, and successively coarsening prior to enrichment, (see next subsection). A regularisation phase is included to optimize the geometrical characteristics, such as neighbour number minimization, segment alignment, maximized circumscribed circle. Dynamical stretching and diagonal swapping are an integral part of the adaptation procedure.

The mesh adaptation criteria follow a shock sensor across adjacent triangles. In this way the moving shocks along the profiles are sensitively captured. Indeed, transient shocks as well as primary shocks are successfully filtered, as can be seen within the different levels of refinement obtained, (see Section 4).

3.2. Non-hierarchical mesh adaptation

The algorithm of the dynamical refinement/derefinement procedure, is based on a certain number of basic algorithmic principles taking into consideration the particularities of local mesh refinement for finite element type generated meshes. Most algorithms of this sort rely on some kind of hierarchical data tree structure.[13-15] This facilitates scanning backwards and forwards via the successive affiliations. This leads to a multi-level programming environment, which can become quite heavy and inhibits structural changes for mesh quality optimization.

Here, a novel anti-data structure has been adopted, where the successive subdivisions are performed independently of the former operations. Firstly, a list of nodes to be invalidated is dressed, followed by their destruction, even if they belong to the initial mesh, i.e. there is no background mesh as with hierarchical methods. Secondly, the remaining configuration is locally refined and optimized to obtain a regular, conformal, admissible mesh. During these stages, a mesh looks like a distribution of nodes. The whole procedure is directly integrated into the flow solver, and by use of dynamical memory management, the updated mesh replaces the former one, with small extra memory allocation. It is not necessary, in this way, to give a maximal overall allocation of memory.

3.3. Algorithm

Three kinds of mesh adaptation can be distinguished: (a) adaptation by moving the points into specific regions where a higher concentration of mesh points is desirable, (b) redistribution of

points within such zones by remeshing, (c) localized refinement by enrichment or derefinement by elimination. In this work, the last possibility is employed. In order to find the specific zones where a higher/lower concentration of mesh points will enhance the accuracy and accelerate convergence, some criteria need to be formulated. There are also three classes of such criteria:

(a) '*a priori*' error estimations, based on the discrete system of governing equations.
(b) '*a posteriori*' error estimations, based upon the Residual, $\mathbf{R}(\mathbf{W}^n)$.
(c) criteria based upon the variations of physical variables.

The complexity of the governing non-linear system of equations renders the first two methods highly complex. However, important advances have been made recently in this domain.[14,16,17] We have adopted the third method in this work, which allows considerable freedom for fixing different tolerances and is well adapted to specific physical phenomena present within the flow fields. For *steady-state* situations we take combinations of $\nabla Mach$, $\nabla Density$ and $\nabla Entropy(s)$, for *unsteady* and *transient* situations combinations of $\Delta Mach$, $\Delta Density$, Δs are taken, where Δ represents differences, and also convected gradients are also useful for wake flows. In fact in the unsteady situation, these criteria are very closely related to the *a posteriori* ones.

Local refinement is obtained by dividing edges at their mid-point, division of elements into 3 is prohibited to avoid obtuse anle situations. Some novel admissibility criteria are enforced to produce regular, conformal and *admissible* triangulations. These are purely geometrical criteria based on the number of neighbours. In particular, in 2D we have that

(i) each candidate for division by 2 must verify

$$\delta^* \geqslant \beta(\delta_1 + \delta_2 + \delta_3)$$

where $0{\cdot}2 \geqslant \beta \geqslant 0{\cdot}3$, δ^* represents the initial edge length, δ_i are the lengths of the three edges of the non-refined triangle otherwise it should be divided by 4.

(ii) It is necessary to ensure that configurations where there are an insufficient or an excessive number of neighbours are avoided. This can be detected by

$$3 \leqslant N_{\text{new edges}} \leqslant 4$$

These two constraints result in a general tendency of 6 neighbours throughout the mesh (in 2D).

(iii) For unsteady flows: never create edges of length smaller than certain tolerance.

3.4. *Optimization*

Once an admissible refinement step has been performed it is necessary to apply optimization rules to obtain smooth, regular, optimally distributed and non-obtuse elements. In the context of the non-hierarchical algorithm presented here, both the refinement and the optimization steps are performed *after* the derefinment one, which is discussed below. Two kinds of optimization methods are developed, geometric ones or ones based upon the actual physics of the flow field.

(1) Geometric optimization is either by
  (a) barycentric and weighted barycentric smoothing
(2) or by structural changes (see Figure 5)
  (b) diagonal swapping via neighbour number rules.

Diagonal swapping is enforced if *one* of the following condition is fulfilled:

$$N_3 + N_4 < N_1 + N_2$$

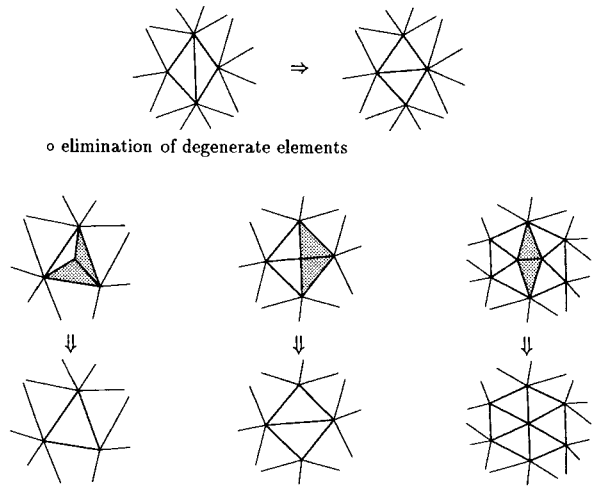

Figure 5. Elimination procedures

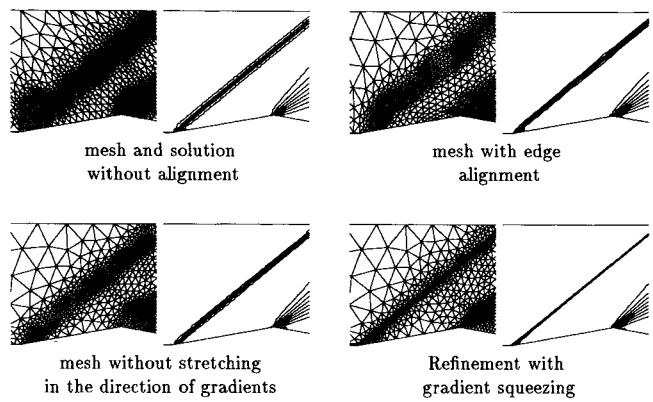

Figure 6. Improvement by aligning segments in the discontinuity direction and local squeezing

$$N_3 + N_4 = N_1 + N_2$$

$$\max(N_3, N_4) < \max(N_1, N_2)$$

(3) Optimization based upon the physics corresponds to
   (a) edge alignment with characteristic directions,
   (b) stretching the node distribution in characteristic directions,
   (c) by further structural changes, (diagonal swapping), alignment with discontinuities is also introduced.

As an example, Figures 6 and 7 show the improvement that can be obtained with these procedures.

A detailed description of all the optimisation procedures can be found in Reference 7 and 18.

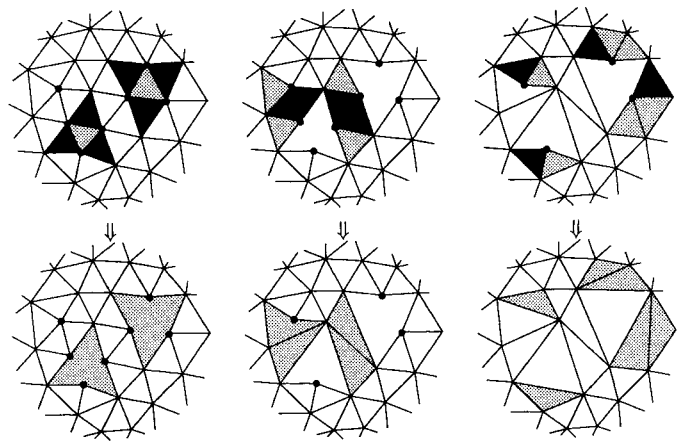

Figure 7. Derefinement algorithm stages with fixed points

3.5. *Mesh derefinement algorithm*

Non-hierarchical Algorithm
- Derefine mesh $\mathcal{M}_{t^n}$
  - Search phase of Fixed points that *cannot* be derefined.
  - singular points, symmetry lines, nodes marked for refinement, etc.
  - Mark nodes that are of key importance (boundaries, and internal)
  - Enter the derefinement phase
- Local refinement phase
  - report criteria to nodes by flagging
  - admissibility
- Optimization $\Rightarrow$ New mesh $\mathcal{M}_{t^n}$
- Calculate solution on this mesh W^{n+1}
- Report criteria depending on W^{n+1}
- Create $M_{t^{n+1}}$ by going back to derefinement step.

The kernel of this phase is the marking of the fixed points. The algorithm is best illustrated by pictures, the fixed points are marked in solid black.

4. NUMERICAL RESULTS

One of the problems considered here is an unsteady supersonic flow at Mach 3 over a forward step, to illustrate the accuracy and efficiency of the hybrid scheme (see Section 2.3). The refinement/derefinement procedure allows a very precise following of the physical properties of the flow field as illustrated with the Figure 4. One-hundred and sixty different meshes where generated overall, for an increase in computational time of approximately 5 per cent.

Another test case which illustrates the power of this algorithm even for steady-state calculations, is that of a supersonic air intake, (Figure 8). Four successive passes of refine-

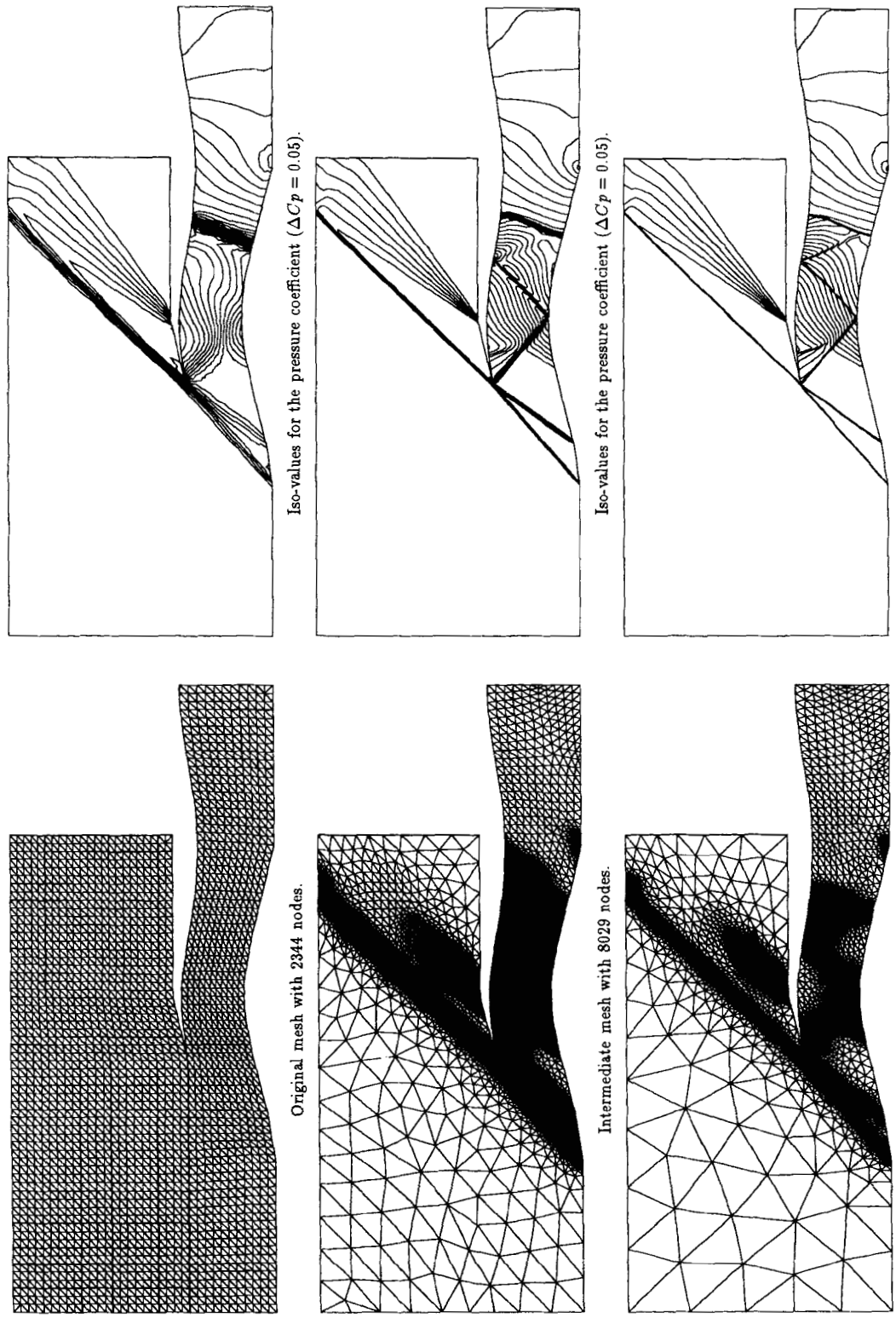

Figure 8. Initial, intermediate and final meshes and corresponding solutions obtained with four passes of dynamic mesh adaption for a supersonique engine air intake

ment/derefinement are used to obtain an extremely precise representation of the flow within the intake for a final mesh of 19 477 nodes. The multiple reflections, and the strong normal shock at the rear of the cowl due to the fixed compressor-entrance pressure are captured with a high degree of precision. Even the small embedded sonic shock can be seen. An equivalent calculation on a structured multi-block mesh needed five times more discretisation points to obtain an equivalent solution.

A transient pitching airfoil case is also illustrated in Figure 9. The aerofoil pitches harmonically about the quarter chord at the semi-chord reduced frequency of $k = 0{\cdot}0814$ and an amplitude of $2{\cdot}51°$. Upstream conditions correspond to $M_\infty = 0{\cdot}755$, with initial angle of attack of $0{\cdot}016°$. The figure illustrates the Iso Cp lines for various angular positions within the complete pitching cycle. The automatic refinement/derefinement is clearly illustrated, with a high precision of the transient shock resolutions. Although the algorithm is totally non-hierarchical with no background mesh, the meshes corresponding to the same point in the cycle are almost equivalent despite the multiple changes that occur during the cycle.

Lastly, a highly unsteady multiple shock reflection problem has been imagined by considering a supersonic flow over the EPFL logo in a duct, Figure 10. The efficiency of the dynamical auto-adaptive mesh algorithm is clearly shown. The physical phenomena illustrated are well captured, from strong shocks, to weak expansions, and weaker secondary shock reflections. The non-hierarchical structure indeed allows more freedom for filtering within the criteria used to detect zones to be refined/derefined. For all the unsteady cases, the difference between two succeeding meshes is small, the structural changes within the optimization phase do not change the positions of the points, there is thus a certain inertia. This could have created problems for the more violently changing flow presented here, but the results are conclusive to the contrary.

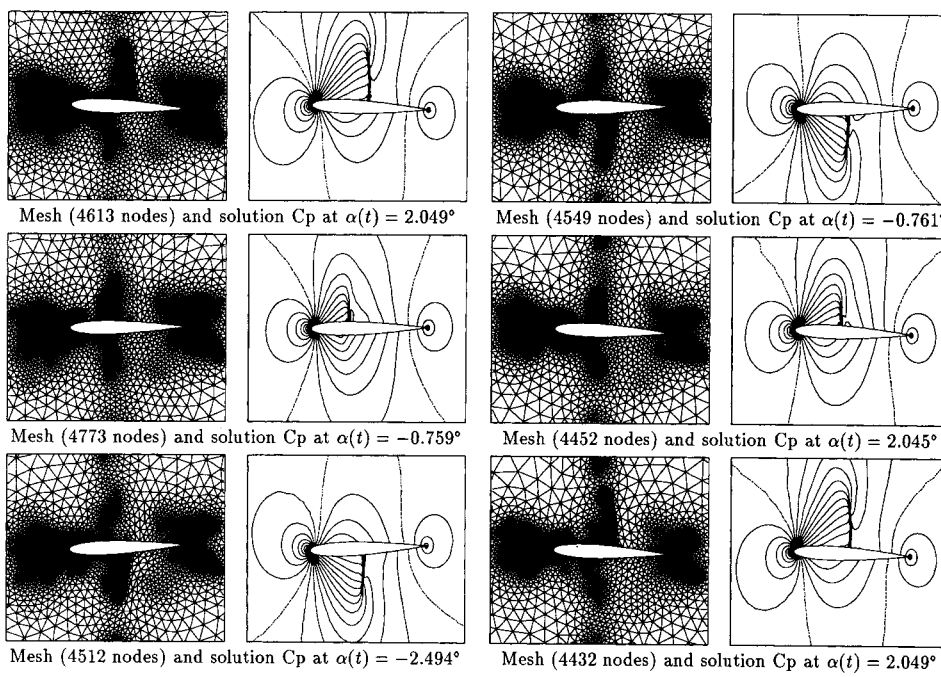

Figure 9. Pitching naca Airfoil with non-hierarchical dynamic adaptation $M_\infty = 0{\cdot}755$, $\alpha_0 = 0{\cdot}016°$, $\alpha_1 = 2{\cdot}51°$, $k = 0{\cdot}0814$

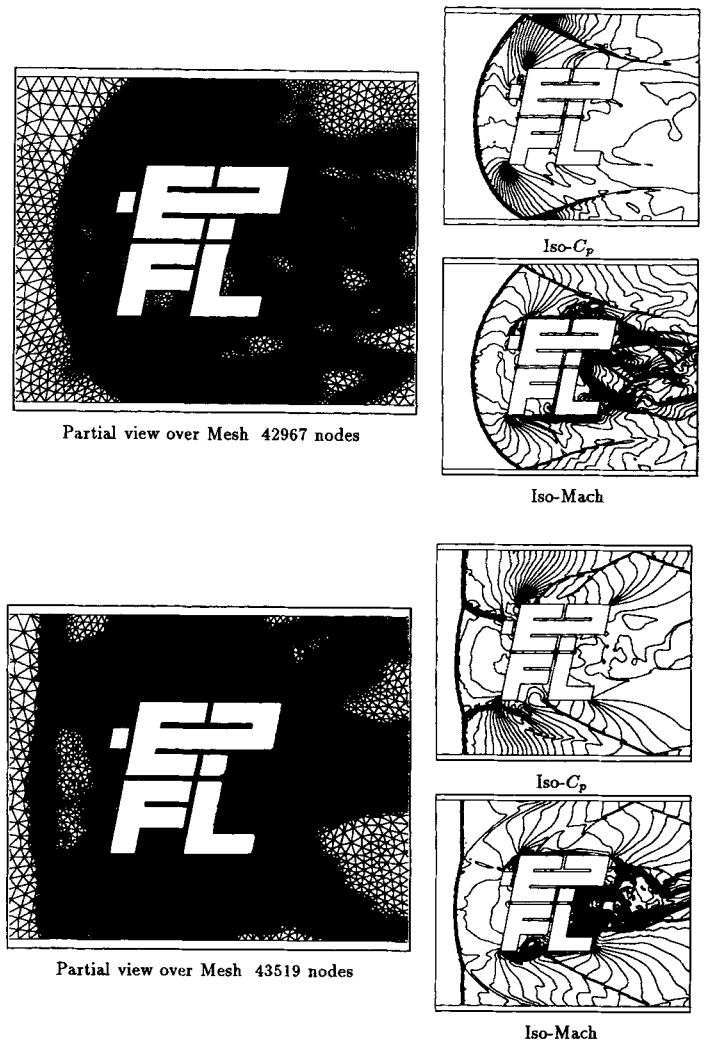

Figure 10. Unsteady flow over EPFL logo—$M_\infty = 3$

5. CONCLUSIONS

Combining entropy corrections for simple solvers gives clearly an interesting alternative to complete Riemann solvers for numerical simulation of many complex unsteady flows. Coupling such a solver with dynamical mesh adaptation by enrichment/coarsening on unstructured meshes provides a considerable enahncement on the accuracy. The novel non-hierarchical dynamical mesh adaptation by refinement/derefinement algorithm provides a robust method for accurate transient and unsteady flow computations, and allows greater freedom for optimizing the quality and precision of the grids. The extension of this work to 3D is under hand and is a promising way of handling complex flow numerics for complex geometries with multiple components.

REFERENCES

1. P. D. Lax, 'Shock waves and entropy', in E. Zarantonello (ed.), *Contribution to Nonlinear Funcational Analysis*, Academic Press, New York, 1971, pp. 603–634.
2. K. Khalfallah, 'Conditions de monotonie et d'entropie et application a une méthode implicite centrée pour les équations d'Euler à grand Mach', *Doctoral thesis*, Université de Paris VI, 1990.
3. P. Woodward and P. Colella, 'The numerical solution of two-dimensional fluid flow with strong shocks', *J. Comput. Phys.*, **54,** 115–173.
4. T. J. R. Hughes, L. P. Franca and M. Mallet, 'A new finite element formulation for computational fluid dynamics: I. Symmetric forms of the compressible Euler and Navier–Stokes equations', *Comput. Methods Appl. Mech. Eng.*, **54,** 223–234 (1986).
5. K. Baba and T. Tabata, 'On a conservative upwind finite element scheme for convective diffusion equations', *RAIRO Numer. Analy.*, **15,** 3–25 (1981).
6. A. Dervieux, VKI Lecture Series, 1984.
7. R. Richter, 'Schémas de capture de discontinuités en maillage non-structuré avec adaptation dynamique', *PhD Thesis*, EPFL, 1993.
8. R. C. Swansen and E. Turkel, 'On central-difference and upwind schemes', *J. Comput. Phys.*, **101,** 292–306 (1992).
9. V. Selmin, *Int. J. Numer. Methods. Sci. Eng.*, 1992.
10. A. Jameson, 'Artificial diffusion, upwind biasing, limiters and their effect on accuracy and multigrid convergence in transonic and hypersonic flows', *AIAA-93-3359.*
11. E. Tadmor, 'The numerical viscosity of entropy stable schemes for systems of conversation laws', *J. Math. Comp.*, **49,** 217–235 (1987).
12. A. Lerat, *Lecture Series 1990-03, Computational Fluid Dynamis*, Von Karman Institute for Fluid Dynamics, Bruxelles, 1990.
13. F. Benkhaldoun, P. Leyland and B. Larrouturou, 'Dynamic mesh adaptation for unsteady nonlinear phenomena—Application to flame propagation', in *Numerical Grid Generation in computational Fluid Mechanics 88*, Sengupta *et al.* (eds.), Miami, 1988, pp. 977–986.
14. P. Leyland, F. Benkhaldoun, N. Maman, B. Larrouturou, 'Dynamical mesh adaptation criteria for accurate capturing of stiff phenomena in combustion', *Int. J . Numer. Methods Heat Mass Transfer*, 1993, to appear.
15. R. Löhner, 'Adaptive remeshing for transient problems', *Comput. Methods Appl. Mech. Eng.*, **75,** 195–214 (1989).
16. C. Johnson, 'Adaptive element methods for diffusion and convection problems', in J. Oden (ed.), *Reliability in Computational Mechanics*, Austin Lakeway, 1989.
17. C. Johnson and A. Szepessy, 'Adaptive finite element methods for conservations laws based on a posteriori error estimates', Preprint Chalmers Univ., 1992–31.
18. R. Richter, 'Discontinuity capturing using auto adaptive finite elements', *Proc. Int. Conf. on Numerical Grid Generation in CFD* Swansea, 6–8 April 1994.